Nanoscale

COMMUNICATION

View Article Online
View Journal | View Issue

Check for updates

Cite this: *Nanoscale*, 2017, **9**, 18590

Received 19th September 2017,
Accepted 5th November 2017

DOI: 10.1039/c7nr07006c

rsc.li/nanoscale

Rocket-inspired tubular catalytic microjets with grating-structured walls as guiding empennages†

Gaoshan Huang, [a] Jiyuan Wang,[b,c] Zhaoqian Liu,[a] Dekai Zhou,[b] Ziao Tian,[a] Borui Xu,[a] Longqiu Li*[b] and Yongfeng Mei *[a]

Controllable locomotion in the micro-/nanoscale is challenging and attracts increasing research interest. Tubular microjets self-propelled by microbubbles are intensively investigated due to their high energy conversion efficiency, but the imperfection of the tubular geometry makes it harder to realize linear motion. Inspired by the macro rocket, we designed a tubular microjet with a grating-structured wall which mimics the guiding empennage of the macro rocket, and we found that the fluid can be effectively guided by the grooves. Both theoretical simulation and experimental work have been carried out, and the obtained results demonstrate that the stability margin of the grating-structured microjet can be enhanced. Compared with microjets with smooth walls, the structured microjets show an enhanced ability of moving linearly. In 10% H_2O_2, only 20% of the smooth microjets demonstrate linear trajectories, while 80% of the grating-structured microjets keep moving straight. The grating-structured microjet can maintain linear motion under external disturbance. We further propose to increase the stability by introducing a helical grating structure.

Inspired by the biomachines of nature, there have been huge efforts towards the development of artificial micro-/nanoscale motors and machines that can mimic the functions of those natural systems, and several kinds of man-made micro-/nanomotors powered by catalytic reactions have so far been realized.[1–11] The locomotion of these motors is normally powered by the conversion of chemical energy from external fuel into mechanical forces, and is achieved through self-electrophoresis, self-diffusiophoresis, or bubble propulsion mechanisms.[4,6,12] Among all those motors, the microjets with a tubular geometry self-propelled by microbubbles have attracted increasing interest and much effort has been devoted to disclosing the underlying mechanism and to explore their potential applications.[4,13–19] Due to their relatively simple motion mechanism and higher motion speed compared with those of rod- and sphere-based motors, their potential applications in the fields of cargo-delivery, environmental remediation, therapeutic treatments, and other biomedical applications are highly expected.[14,18,20] To meet the demands of these applications, steering of the microjets towards a specific destination and controlling their motion speeds will be required.[14,20] For tubular microjets, the speed can be easily controlled by altering the concentrations of chemicals,[13,14] introducing the surface fine structures,[21–23] or designing a biomimetic interface,[24] and thus the gas production rate in the chemical reactions can be tuned correspondingly. The direction steering is commonly achieved by an external magnetic field but magnetic materials need to be incorporated in advance.[25–28] However, a few factors make the direction steering difficult to be achieved. In such a small scale, the Brownian motion becomes significant, and the influence from the viscous force is large (*i.e.*, low Reynolds number).[14,20] In addition, the geometries of the microjets may also influence their motion behaviors. The so-called rolled-up technology utilizes the intrinsic strain gradients inside the nanomembranes to assemble the microtubes.[4,29–36] This strategy has been widely used to produce tubular microjets due to the easy fabrication route and the convenient introduction of materials in the form of multi-layered structures.[4,30] Unfortunately, the self-assembly commonly leads to imperfection in the tubular geometry and the tube opening may not be ideally circular. The expelling of the bubble may deviate from the longitudinal axis of the microtube, resulting in various motion trajectories rather than linear motion.[14,35,37] The excitation of eddy flow during the movement was also found to disturb the linear motion.[38] The precise motion control of the microjet is there-

[a]*Department of Materials Science, State Key Lab of ASIC and System, Fudan University, Shanghai 200433, P. R. China. E-mail: yfm@fudan.edu.cn*
[b]*Key Laboratory of Micro-systems and Micro-structures Manufacturing of Ministry of Education, Harbin Institute of Technology, Harbin 150001, P. R. China. E-mail: longqiuli@hit.edu.cn*
[c]*School of Electrical and Control Engineering, Heilongjiang University of Science and Technology, Harbin 150022, P. R. China*

† Electronic supplementary information (ESI) available: Detailed calculations of the dynamics of microjet with grating-structured wall, and microjet with helical grating structure; typical motions of grating-structured and smooth microjets; interaction between a grating-structured microjet and a bubble in the fluid. See DOI: 10.1039/c7nr07006c

fore still challenging because even the linear motion cannot be guaranteed. In such circumstances, we expect to realize stabilized linear motion *via* sophisticated structural optimization.

We noticed that fishes use their fins to control their movement directions. Similarly, man-made submarines, torpedoes, and rockets, which can be considered the macro counterparts of the microjet, normally have guiding empennages to steer the motion directions. Fig. 1a shows a model of a macro rocket, in which the empennage located at the rear part can be used to guide the air flow, and the motion of the rocket is stabilized even at high speeds. This enlightens us to control the motion direction of the microjet with a similar empennage-like structure. But fabricating such micro empennages may not be easy especially for rolled-up tubular microjets which are produced by self-assembly processes. Fortunately, our group has recently developed a convenient method to fabricate rolled-up structures with grating-structured walls.[39] We considered that when the structured microjets move in the solution, the grating structure on the wall can be used as grooves to guide the fluid flow (Fig. 1b). The effect of the grating structure is therefore similar to that of the guiding empennage in the macro rocket, and stabilized linear motion can be achieved. In the present work, we analyzed the dynamics of the grating-structured microjet. Both theoretical and experimental results prove that the stability margin of such microjets can be largely enhanced compared with that of microjets with smooth walls, and stabilized linear motion of microjets was observed. The microjets can maintain their linear motion even under external disturbance. The influence of the orientation angle of the grating with respect to the tube axis was also discussed. The results in this work may give a clue on steering the motion of the microjet without an external field and thus may have potential applications in many fields such as drug delivery,[40,41] isolation of biological targets,[42] and environmental remediation,[43] where the ability to maintain the linear motion towards the targets is crucial.

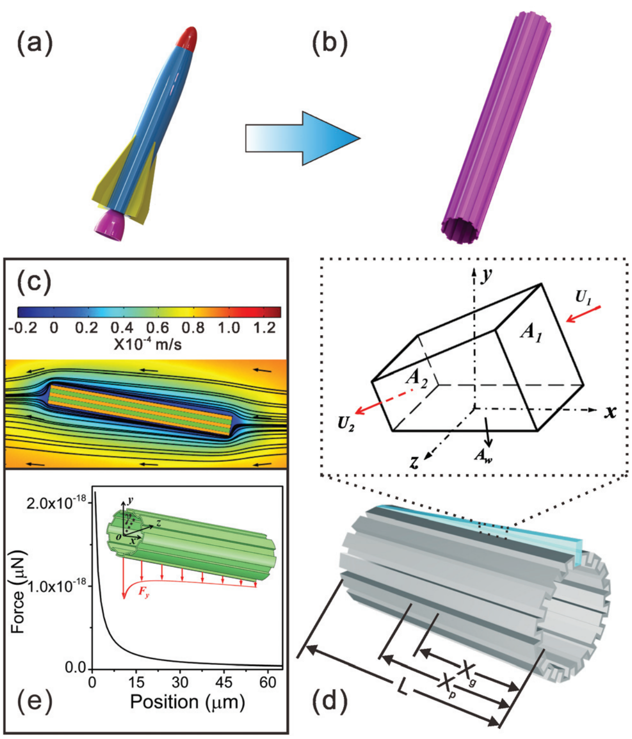

Fig. 1 (a) Model of a macro rocket. (b) Diagram of a tubular microjet with a grating-structured wall. (c) Nephogram of flow speed distribution. The microjet is considered to be static while the fluid flows towards the microjet. (d) Diagram of a grating-structured microjet with the fluid in one groove (streamtube) highlighted. The upper panel shows the infinitesimal element used for the theoretical calculation. (e) Forces (per micrometer) along the microjet produced by the pressure from the fluid. The inset shows the corresponding schematic diagram.

For a grating-structured microjet moving in a fluid, a theoretical model is established to analyze its dynamics. In this model, for the sake of clarity, we choose the frame of reference attached to the microjet. Thus the microjet is considered to be static while the fluid flows towards the microjet. Here, the microjet is considered to move with a uniform speed. The orientation of the microjet is suddenly changed due to an external disturbance, and thus a tilt angle θ between the longitudinal axis of the microjet and the flow velocity vector of the fluid is produced. In this case, the flow speed of the liquid/fluid surrounding the microjet was simulated (COMOSOL Multiphysics software), and the obtained nephogram of the flow speed is shown in Fig. 1c. The nephogram demonstrates that the flow at the approaching side is compressed (see the upper-left part of Fig. 1c) when there is a tilt angle θ between the longitudinal axis of the microjet and the flow velocity vector (*i.e.*, moving direction of the microjet). Due to the existence of the grating structure (*i.e.*, the grooves) on the tube wall, the fluid that flows through the groove forms a streamtube, and is constrained by the groove. The fluid flowing in one groove is highlighted in Fig. 1d and S1† for further investigation, and an arbitrary infinitesimal element with the control volume is specified in the upper panel. The fluid flows into the infinitesimal element from the section A_1 and outflows from section A_2. Clearly, the area of A_1 is larger than that of A_2 due to the angle θ. According to the continuity equation of fluid dynamics, the flow speed at A_1 (U_1) is smaller compared with the flow speed at A_2 (U_2). On the other hand, the flow speed on the side (A_w) of the infinitesimal element is zero, because it is a non-penetrable surface. According to the Bernoulli equation and the conservation of momentum,[44,45] the pressure of the fluid on the bottom of the groove changes with the flow speed, and forces are generated correspondingly. For a groove with an azimuthal angle γ (see the inset of Fig. 1e and Fig. S2†), the component of the force along the y direction $F_{y,\gamma}$ can be written as

$$F_{y,\gamma} = -\rho {U_1}^2 A_1 \sin\theta\cos\gamma + \frac{\rho {U_1}^2}{2}\left[1+\left(\frac{A_1}{A_2}\right)^2\right] A_2 \sin\theta\cos\gamma, \tag{1}$$

where ρ is the density of the fluid (detailed calculation can be found in the ESI†). For all the grooves on the wall of a microjet, the resultant force F_y should be:

$$F_y = \sum_{\gamma} \int_0^L F_{y,\gamma} \mathrm{d}x. \tag{2}$$

The force distribution along the microjet is demonstrated in Fig. 1e, and the inset of Fig. 1e shows a corresponding schematic diagram. One can see that the forces are not uniform: the forces are smaller in the front part and larger in the rear part. The moment generated can restore the original motion direction, which suggests that a stable linear motion is easier to be achieved in the case of the grating-structured microjet. To quantitatively evaluate the stability of the microjet, a parameter named static stability margin (T) can be defined as[46,47]

$$T = \frac{x_\mathrm{p} - x_\mathrm{g}}{L} \times 100\%, \tag{3}$$

where x_p is the position of the action point of the resultant force F_y from the fluid pressure, which can be calculated by using the equation

$$x_\mathrm{p} = \frac{\sum\limits_{\gamma} \int_0^L F_{y,\gamma} x \mathrm{d}x}{\sum\limits_{\gamma} \int_0^L F_{y,\gamma} \mathrm{d}x}, \tag{4}$$

where x_g is the position of the center of mass,[48] and L is the length of the microjet, as shown in Fig. 1d (detailed calculation can be found in the ESI†). A larger T indicates that the linear motion can be easily restored when the motion of the microjet is disturbed by *e.g.*, a random turbulence. In the present case, we indeed found that the stability margin can be remarkably enhanced in the grating-structured microjet. To calculate the stability margin quantitatively, we used the geometrical parameters from the experiment, and the comparison between theoretical and experimental works will be discussed.

Experiments were carried out to prove the feasibility of using the grating structure on the tube wall to control the locomotion. To fabricate such a microtube with a fine structure, a process combining conventional photolithography and laser interference lithography was engaged, as shown in Fig. 2a. Briefly, a layer of ARP-3510 photoresist (All-resist GmbH) was deposited on a Si wafer by spin-coating, and the thickness of the photoresist layer is measured to be ~2 μm.[49] The photoresist layer was then patterned into different shapes (*e.g.*, circular shape) by conventional photolithography. After this step, a grating structure was introduced by laser interference lithography (step i in Fig. 2a), where a He–Cd laser with a wavelength of 325 nm and a power of 5 mW was used as a light source, and the periodicity of the grating structure could be tuned between 1 and 9 μm. This grating-structured photoresist layer (step i in Fig. 2a) was used as a sacrificial layer and a pre-strained Ti/Cr/Pt tri-layer with a thickness of 7/7/6 nm was deposited onto the sacrificial layer by e-beam evaporation at 2×10^{-4} Pa (step ii in Fig. 2a). Here, the Ti/Cr

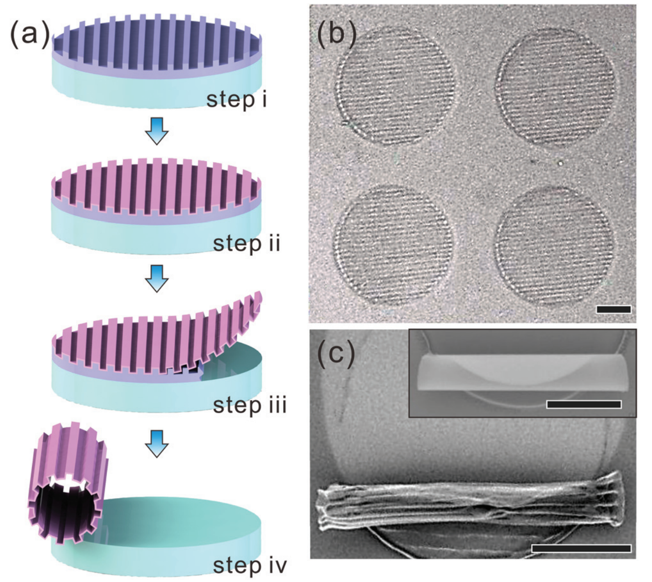

Fig. 2 (a) Three-dimensional schematic illustration of the fabrication process of the microtube with a grating-structured tube wall (from step i to step iv). (b) Optical microscopy image of the photoresist sacrificial layer with a periodic grating structure. Scale bar: 20 μm. (c) A typical morphology of a grating-structured microtube. The inset shows a SEM image of a smooth microtube for comparison. Scale bars: 20 μm.

was deposited at different rates (1 Å s^{-1} and 0.1 Å s^{-1} respectively) to build the strain gradient along the vertical direction for the subsequent rolling-up process and Pt was used as a catalyst for H_2O_2 decomposition.[22] In the next step (step iii in Fig. 2a), the underetching of the sacrificial photoresist layer was conducted by putting the sample in acetone. The photoresist was removed and the metallic trilayer was set free to self-assemble into a tubular structure (step iv in Fig. 2a). The sample was then dried in a critical point dryer (Leica CPD 030) for the following experiment. For comparison, we also prepared a microtube with a smooth wall. The fabrication process was similar: only the laser interference lithography step was skipped.

Fig. 2b shows an optical microscopy image of a grating-structured photoresist sacrificial layer before the deposition of a metallic trilayer. The diameter of the circular patterns defined by conventional photolithography is 65 μm and the grating structure with a periodicity of ~2.5 μm can be observed. Fig. 2c shows a scanning electron microscopy (SEM) image of a typical microtube fabricated in our experiment with a grating structure, which proves that the grating structure in the photoresist layer was successfully transferred to the tube wall. The diameter of the microtube is ~8 μm and the width and the depth of the grooves on the tube wall are estimated to be ~1.5 and ~0.5 μm respectively. The inset in Fig. 2c shows a SEM image of a smooth microtube with a similar diameter. We also notice in our experiment that the rolling direction of the structured nanomembrane is basically perpendicular to the fringes of the grating structure. The phenomenon is ascribed to the anisotropy introduced by the grating structure.[39] Previous literature about the rolling should kinetically favor this preferential rolling direction to minimize the elasticity energy.[50] This enables the disclosure of the motion behavior of the grating-structured microjet, as we use this geometrical configuration in the theoretical model (see Fig. 1). However, a small deviation from this preferential rolling direction could exist in the experiment. Its influence on the motion of the microjet will be discussed later.

Previous investigation shows that the motion trajectories of the tubular microjets can be diverse, mainly due to the imperfection of the tubular geometries.[35,37] The expelling of the microbubbles may deviate the direction of the tube axis in this case. In addition, the existence of the eddy flow, especially in the case of high-speed motion, also disturbs the straight motion.[38] In general, the motion behaviors can be classified into two groups. First, linear or quasi-linear motion: the curvature radii of the trajectories >3000 μm, which is much larger than the length of the microjet. Second, circular or spiral motion where the curvature radius is comparable to the length of the microjet. The insets of Fig. 3a show typical trajectories of these two motion behaviors (see also ESI Movie 1†). To study the influence of the grating structure on the motion behaviors in detail, we prepared microjets with smooth and structured tube walls, and analyzed their motion behaviors in H_2O_2 solutions with different concentrations. For each H_2O_2 concentration, we counted trajectories of at least 20 microjets (for both smooth and structured cases), and the percentage of linear or quasi-linear trajectories was calculated, as shown in Fig. 3a. We notice that among microjets with similar geometries and motion speeds, the grating-structured microjets demonstrate a visibly high ability of moving straight. The difference is even remarkable in fuel with higher H_2O_2 concentration. In 10% H_2O_2, only 20% of the smooth microjets demonstrate linear trajectories, while 80% of the structured microjets keep moving straight, indicating that the grating structures on the tube walls can effectively stabilize the linear motion. On the basis of the aforementioned model (Fig. 1c–e), we calculated the static stability margin and the moment from the fluid flow by using θ as a parameter, and the calculated results are shown in Fig. 3b, where the geometrical parameters were derived from the experimental results. One can see that both the static stability margin and the moment from the fluid flow increase with θ. The large moment from the field results in the microjet rotating back to the movement direction, which means that the stabilizing effect of the grating structure becomes evident for a large θ. This is also consistent with the experimental results shown in Fig. 3a. Another noteworthy experimental phenomenon is that the percentages of linear trajectories decrease with increasing H_2O_2 concentration for two kinds of microjets although most structured microjets can move straight. We consider this to be mainly due to the circular flow around the microtube (see the diagram in the inset of Fig. 3c) and the corresponding drag force F produced. Here, the drag force F perpendicular to the tube axis was calculated

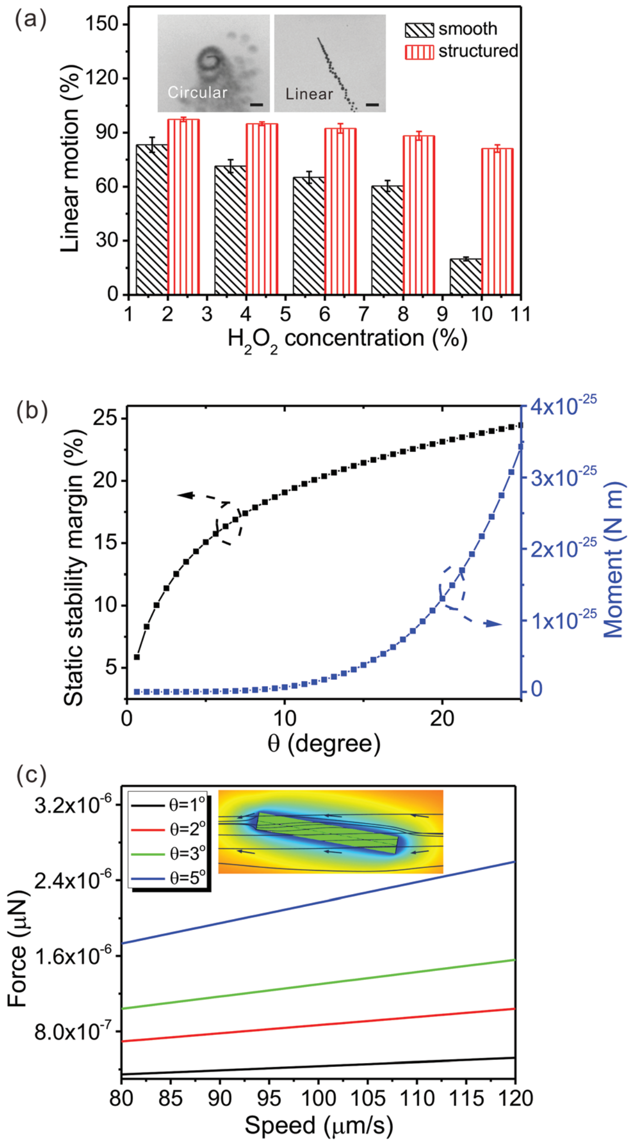

Fig. 3 (a) Statistics of the motion behaviors of the tubular microjets with smooth and grating-structured walls. The histograms show the percentages of the microjets moving with linear trajectories in different H_2O_2 concentrations. The insets show two typical motion trajectories: linear (left) and circular/spiral (right). Scale bars: 100 μm. (b) The evolvement of the static stability margin and the moment from the flow as a function of the angle θ. The data are extracted from the calculation based on the model in Fig. 1. (c) Drag force due to the circular flow around the microtube as a function of the motion speed. The plots show the dependences for different angles. The inset shows the model used in the theoretical calculation and the flow of the fluid is schematically demonstrated. In the theoretical model, the length and the diameter of the microjet are 65 and 8 μm respectively while the width and the depth of the groove are 1.5 and 0.5 μm respectively.

theoretically by considering the radial component of the flow field:[51]

$$F = \frac{4\pi\mu L \sin\theta}{\ln\frac{L}{R} + 0.5} U, \tag{5}$$

where μ is the fluid viscosity, R is the radius of the microtube, and U is the motion speed. The obtained results are shown in Fig. 3c. The results illustrate that the drag force should be linearly proportional to the motion speed U. Since the force makes the microtube rotate away from the original direction and the force increases with θ (Fig. 3c), a small deviation due to a random disturbance will be further "amplified" by continuous rotation and thus the linear motion can hardly be maintained. Consequently, the percentage of linear motion decreases with the motion speed, as observed experimentally in Fig. 3a. Although this factor exists for all tubular microjets, the influence can be partly balanced in those with grating structures due to the stabilizing effect, and therefore, more linear trajectories can be realized.

In previous studies by our group, a meniscus-climbing behavior mimicking water-walking insects was observed and investigated.[52,53] It was demonstrated that a lateral capillary force existed between small floating objects and the force could attract objects over a distance comparable to the capillary length.[52–54] The moving microjets were always attracted by the meniscus-effect at the borders of bubbles in the fluid. The moving direction was influenced by the capillary force which acted as a centripetal force and then the microjet held a circular motion.[52] In the present case, we noticed that sometimes the microjet with a grating-structured wall could escape from this attraction effect. A typical experimental observation in 1.5% H_2O_2 is shown in Fig. 4a (see also ESI Movie 2†). The microjet changes its direction to move around the bubble for nearly a semi-circumference and then escapes from the interaction. The linear motion is restored after that. This phenomenon was observed repeatedly in our experiments. It seems that the influence from the capillary force in the present case is trivial compared to that in the case of a smooth microjet.[52] We consider that there may be at least two factors contributing to this difference. Firstly, as mentioned above, the stability margin of the grating-structured microjet will help the microjet to move linearly, which can partially reduce the influence from the capillary force. Secondly, as the surface of the structured microjet is no longer smooth, the radius of the contact line may decrease,[55,56] and the capillary force decreases correspondingly.[57] The co-effect of these two factors thus leads to the experimental observation shown in Fig. 4 and ESI Movie 2.† However, in the case

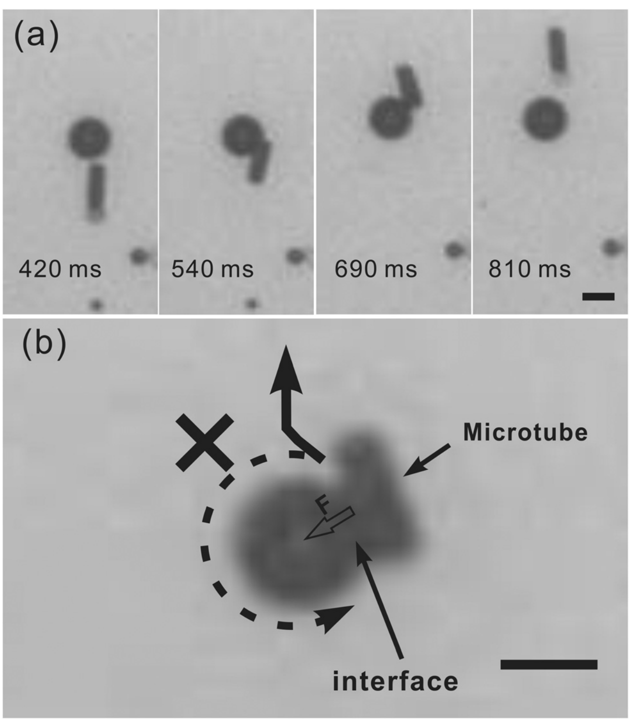

Fig. 4 (a) Time-lapse images of a grating-structured microjet encountering a bubble in the fluid. (b) Enlarged image demonstrating the interaction between the microjet and the bubble. Scale bars: 50 μm.

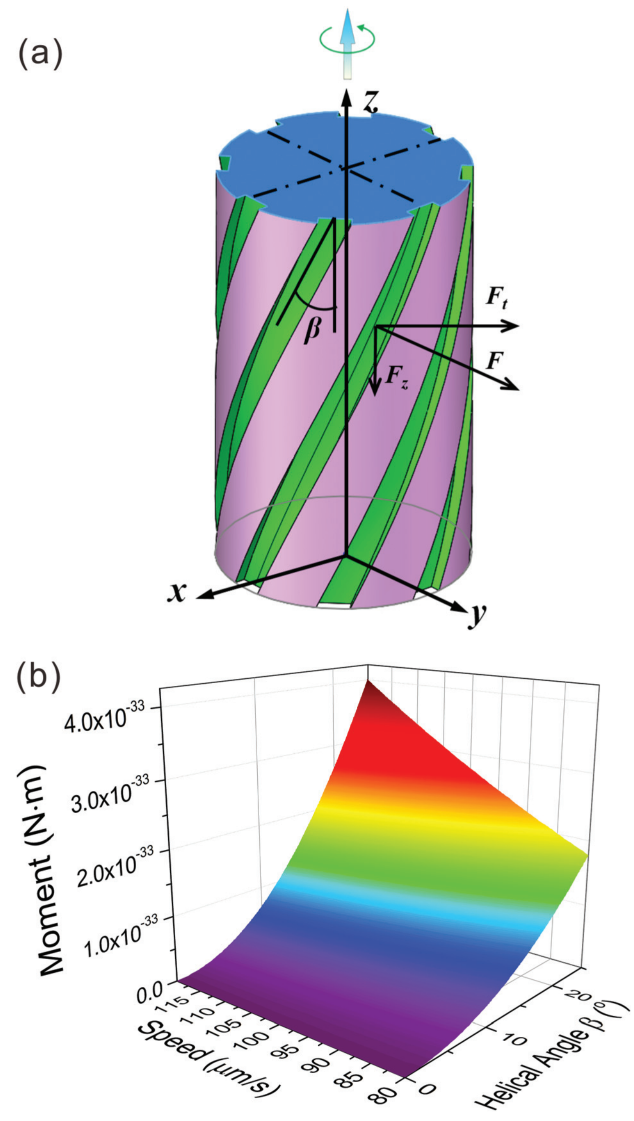

Fig. 5 (a) Diagram of a tubular microjet with a helical grating structure on the wall. The force produced by the fluid is briefly demonstrated. The spin of the microjet is schematically shown. (b) The moment produced by the tangential force (F_t) as a function of motion speed and helical angle β.

of the smooth microjet, neither factor existed. Thus the smooth microjets were always attracted by the bubbles.

Finally, we would like to briefly discuss more about the misalignment between the orientation of the grating structure and the longitudinal axis of the microjet. In a real case, the orientation of the grating may not be perfectly parallel to the axis of the microtube as supposed in the theoretical model (Fig. 1), and an included angle β can be defined as shown in Fig. 5a. In such a case, the flow of the fluid in the grooves produces force F, whose tangential component F_t and corresponding moment M_t cause the rotation/spin of the microjet around its axis, as shown schematically in Fig. 5a. On the basis of this model, we analyzed the dynamics of such a microjet with a helical grating structure theoretically (ESI†), and the obtained results are shown in Fig. 5b. One can see that the moment of the tangential force increases with the speed of the microjet and the helical angle β. In addition, we consider the microjet with spin as an analogue of a gyroscope, where the rotation axis maintains its original orientation due to the conservation of angular momentum and the Coriolis effect.[58] Thus the stability of the locomotion of the microjet with the helical grating structure can be further enhanced. More experimental work on this aspect will be carried out in the future.

Conclusions

In conclusion, inspired by the fins of fish and the empennages of rockets, torpedoes, and submarines, we designed a rolled-up tubular microjet with a grating-structured wall. Compared to the smooth microjet, the grating structure and the corresponding grooves can guide the flow of the fluid during the self-propelled motion. If the motion direction is tilted, the fluid constrained by the grooves can apply a force on the wall of the microjet to restore the original direction. Theoretical calculations further prove that an enhanced static stability margin can be produced in such a case and experimental observations prove that grating-structured microjets have a greater possibility of moving straight compared with the smooth microjets. The stability margin can even restore the linear motion after an external disturbance. The misalignment between the grating structure and the tube axis produces helical grooves which may further improve the motion stability. The current fabrication approach based rolled-up technology provides a convenient way to parallelly produce microjets with a designed microstructure, which can be used to optimize the controllable locomotion in the micro-/nanoscale. We believe that this kind of microjet with grating-structured walls may have important potential in biomedical applications such as drug delivery and isolation of biological targets, because many disturbances exist in the *in vivo* environment and reaching the destination accurately should be crucial.

Conflicts of interest

There are no conflicts to declare.

Acknowledgements

This work was supported by the National Natural Science Foundation of China (No. 51475093, 51521003, 51711540298, and U1632115), Science and Technology Commission of Shanghai Municipality (no. 17JC1401700), and the Changjiang Young Scholars Programme of China. J. Wang, D. Zhou and L. Li are grateful for the financial support from Key Laboratory of Micro-systems and Micro-structures Manufacturing of Ministry of Education (2016KM004) and Self-Planned Task of State Key Laboratory of Robotics and System (HIT) (SKLRS 201706A).

References

1 T. L. Xu, W. Gao, L. P. Xu, X. J. Zhang and S. T. Wang, *Adv. Mater.*, 2017, **29**, 1603250.
2 G. A. Ozin, I. Manners, S. Fournier-Bidoz and A. Arsenault, *Adv. Mater.*, 2005, **17**, 3011.
3 M. Guix, C. C. Mayorga-Martinez and A. Merkoci, *Chem. Rev.*, 2014, **114**, 6285.
4 Y. F. Mei, A. A. Solovev, S. Sanchez and O. G. Schmidt, *Chem. Soc. Rev.*, 2011, **40**, 2109.
5 J. Wang, *ACS Nano*, 2009, **3**, 4.
6 W. Wang, W. T. Duan, S. Ahmed, T. E. Mallouk and A. Sen, *Nano Today*, 2013, **8**, 531.
7 S. Sanchez, L. Soler and J. Katuri, *Angew. Chem., Int. Ed.*, 2015, **54**, 1414.
8 K. Kim, J. Guo, X. Xu and D. L. Fan, *Small*, 2015, **11**, 4037.
9 Y. F. Ru, F. Peng, X. F. Sui, Y. J. Men, P. B. White, J. C. M. van Hest and D. A. Wilson, *Nat. Chem.*, 2017, **9**, 480.
10 J. X. Li, P. Angsantikul, W. J. Liu, B. E. F. de Avila, S. Thamphiwatana, M. L. Xu, E. Sandraz, X. L. Wang, J. Delezuk and W. W. Gao, *Angew. Chem., Int. Ed.*, 2017, **56**, 2156.
11 A. Sen, *Nat. Nanotechnol.*, 2016, **11**, 1003.
12 M. Pumera, *Nanoscale*, 2010, **2**, 1643.
13 J. X. Li, G. S. Huang, M. M. Ye, M. L. Li, R. Liu and Y. F. Mei, *Nanoscale*, 2011, **3**, 5083.
14 G. S. Huang, J. Wang and Y. F. Mei, *J. Mater. Chem.*, 2012, **22**, 6519.
15 L. Q. Li, J. Y. Wang, T. L. Li, W. P. Song and G. Y. Zhang, *Soft Matter*, 2014, **10**, 7511.
16 J. X. Li, W. J. Liu, J. Y. Wang, I. Rozen, S. He, C. R. Chen, H. G. Kim, H. J. Lee, H. B. R. Lee, S. H. Kwo, T. L. Li, L. Q. Li, J. Wang and Y. F. Mei, *Adv. Funct. Mater.*, 2017, **27**, 1700598.
17 B. R. Xu and Y. F. Mei, *Sci. Bull.*, 2017, **62**, 525.
18 J. X. Li, I. Rozen and J. Wang, *ACS Nano*, 2016, **10**, 5619.
19 G. Zhao, B. Khezri, S. Sanchez, O. G. Schmidt, R. D. Webster and M. Pumera, *Chem. Commun.*, 2013, **49**, 9125.
20 W. Z. Teo and M. Pumera, *Chem. – Eur. J.*, 2016, **22**, 14796.

21 J. X. Li, J. Zhang, W. Gao, G. S. Huang, Z. F. Di, R. Liu and Y. F. Mei, *Adv. Mater.*, 2013, **25**, 3715.
22 J. X. Li, Z. Q. Liu, G. S. Huang, Z. H. An, G. Chen, J. Zhang, M. L. Li, R. Liu and Y. F. Mei, *NPG Asia Mater.*, 2014, **6**, e94.
23 C. Jiang, G. S. Huang, S. J. Ding, H. L. Dong, C. L. Men and Y. F. Mei, *Nanoscale Res. Lett.*, 2016, **11**, 289.
24 X. C. Chang, L. Q. Li, T. L. Li, D. K. Zhou and G. Y. Zhang, *RSC Adv.*, 2016, **6**, 87213.
25 W. Gao, S. Sattayasamitsathit, J. Orozco and J. Wang, *J. Am. Chem. Soc.*, 2011, **133**, 11862.
26 D. Kagan, S. Campuzano, S. Balasubramaanian, F. Kuralay, F. U. Flechsig and J. Wang, *Nano Lett.*, 2011, **11**, 2083.
27 S. Sanchez, A. A. Solovev, S. Schulze and O. F. Schmidt, *Chem. Commun.*, 2011, **47**, 698.
28 A. A. Solovev, S. Sanchez, M. Pumera, R. F. Mei and O. F. Schmidt, *Adv. Funct. Mater.*, 2010, **20**, 2430.
29 O. G. Schmidt and K. Eberl, *Nature*, 2001, **410**, 168.
30 Y. F. Mei, G. S. Huang, A. A. Solovev, E. Bermúdez Ureña, I. Mönch, F. Ding, T. Reindl, R. K. Y. Fu, P. K. Chu and O. F. Schmidt, *Adv. Mater.*, 2008, **20**, 4085.
31 Z. A. Tian, L. N. Zhang, Y. F. Fang, B. R. Xu, S. W. Tang, N. Hu, Z. H. An, Z. Chen and Y. F. Mei, *Adv. Mater.*, 2017, **29**, 1604572.
32 X. Y. Lin, Y. F. Fang, L. J. Zhu, J. Zhang, G. S. Huang, J. Wang and Y. F. Mei, *Adv. Opt. Mater.*, 2016, **4**, 936.
33 H. Wang, H. L. Zhen, S. L. Li, Y. L. Jing, G. S. Huang, Y. F. Mei and W. Lu, *Sci. Adv.*, 2016, **2**, e1600027.
34 Z. Chen, G. S. Huang, I. Trase, X. M. Han and Y. F. Mei, *Phys. Rev. Appl.*, 2016, **5**, 017001.
35 K. Yao, M. Manjare, C. A. Barrett, B. Yang, T. T. Salguero and Y. Zhao, *J. Phys. Chem. Lett.*, 2012, **3**, 2204.
36 V. Magdanz, G. Stoychev, L. Ionov, S. Sanchez and O. G. Schmidt, *Angew. Chem., Int. Ed.*, 2014, **53**, 2673.
37 A. A. Solovev, Y. F. Mei, E. Bermúdez Ureña, G. S. Huang and O. G. Schmidt, *Small*, 2009, **5**, 1668.
38 S. Sanchez, A. N. Ananth, V. M. Fomin, M. Viehrig and O. F. Schmidt, *J. Am. Chem. Soc.*, 2011, **133**, 14860.
39 T. Huang, Z. Q. Liu, G. S. Huang, R. Liu and Y. F. Mei, *Nanoscale*, 2014, **6**, 9428.
40 J. Wang, *Lab Chip*, 2012, **12**, 1944.
41 D. Patra, S. Sengupta, W. Duan, H. Zhang, R. Pavlik and A. Sen, *Nanoscale*, 2013, **5**, 1273.
42 J. Wang and W. Gao, *ACS Nano*, 2012, **6**, 5745.
43 J. G. S. Moo and M. Pumera, *Chem. – Eur. J.*, 2015, **21**, 58.
44 F. M. White, *Fluid Mechanics*, McGraw-Hill, 2003, pp. 135–185.
45 G. K. Batchelor, *An Introduction to Fluid Dynamics*, Cambridge University Press, 2002, pp. 141–265.
46 H. V. de Castro, *The Longitudinal Static Stability of Tailless Aircraft, 0018/1*, Cranfield University, 2001.
47 J. Bazile, *Prog. Flight Dyn. GNC Avioincs*, 2013, **6**, 17.
48 J. Bazile, *US Pat*, US8265802B2, 2012.
49 G. S. Huang, Y. F. Mei, D. J. Thurmer, E. Coric and O. F. Schmidt, *Lab Chip*, 2009, **9**, 263.
50 P. Cendula, S. Kiravittaya, I. Mönch, J. Schumann and O. G. Schmidt, *Nano Lett.*, 2011, **11**, 236.
51 R. G. Cox, *J. Fluid Mech.*, 1970, **44**, 791.
52 J. X. Li, B. R. Lu, Z. K. Shen, Z. C. Xu, H. Li, J. J. Wen, Z. D. Li, X. P. Qu, Y. F. Chen, Y. F. Mei and R. Liu, *Microelectron. Eng.*, 2011, **88**, 1792.
53 A. A. Solovev, Y. F. Mei and O. G. Schmidt, *Adv. Mater.*, 2010, **22**, 4340.
54 J. W. M. Bush, D. L. Hu and M. Prakash, *Adv. Insect Physiol.*, 2008, **34**, 118.
55 R. N. Wenzel, *J. Phys. Chem.*, 1949, **53**, 1466.
56 M. S. Bell, A. Shahraz, K. A. Fichthorn and A. Borhan, *Langmuir*, 2015, **31**, 6752.
57 P. A. Kralchevsky and K. Nagayama, *Adv. Colloid Interface Sci.*, 2000, **85**, 145.
58 C. Fu, O. Elmazria, F. Sarry, T. Mahalingam, S. S. Yang and K. Lee, *Sens. Actuators, A*, 2014, **220**, 270.

